Limnol. Oceanogr., 55(2), 2010, 481–491

Inorganic carbon and biological oceanography above a shallow oxygen minimum in the entrance to the Gulf of California in the Mexican Pacific

Helmut Maske,[a,*] Ramón Cajal Medrano,[b] Armando Trasviña Castro,[a] Alejandrina Jiménez Mercado,[b,1] Cesar O. Almeda Jauregui,[a] Gilberto Gaxiola Castro,[a] and José Ochoa[a]

[a] Centro de Investigación Científica y de Educación Superior de Ensenada, Ensenada, Baja California, Mexico
[b] Universidad Autónoma de Baja California, Facultad de Ciencias Marinas, Ensenada, Baja California, Mexico

Abstract

The eastern Pacific intermediate oxygen minimum layer (OML) is particularly well-developed and shoals close to the Mexican coast. We obtained hydrographic profiles including oxygen concentration [O], measured dissolved inorganic carbon (DIC), continuous surface pCO_2 in water and air and took biological data south of the Gulf of California in March 2005. The core of the OML, with close to zero [O] was centered around 475 m with a thickness of the core varying between 80 m and 700 m and the upper limit of the core ranging from 500 m to 80 m. At the surface [O] was close to air-saturation and showed no relation with the depth of the OML contrary to DIC and pCO_2 concentrations. Below 50-m depth the changes in DIC and Apparent Oxygen Utilization (AOU) yielding a molar ratio of $\delta DIC = 0.79 \times \delta AOU$. When the OML shoaled, surface temperature, chlorophyll concentration [CHL], and depth-integrated zooplankton increased, resulting in positive correlations among plankton biomass, pCO_2, and DIC in surface waters. When [CHL] is recalculated as particulate organic carbon (POC), a linear relationship with the sum of DIC and POC is observed as expected for concomitant transport of DIC and inorganic nutrients supporting POC formation. Neglecting ventilation of carbon into the atmosphere and the production of dissolved organic carbon, the results suggested that ~ 16% of the carbon transported up from the OML was present in surface waters in the form of POC and the rest in inorganic form.

In the subtropical and tropical eastern Pacific intermediate oxygen minimum layers (OML) are present in the water column. Oxygen minimum layers within the oceanographic water column and dead zones close to the sediment have recently met with heightened interest partly because of the tendency to increase in frequency or extend, possibly forced by anthropogenic factors (Chan et al. 2008; Diaz and Rosenberg 2008; Oschlies et al. 2008) and partly because of their influence on biology. The OML in the subtropical Mexican Pacific is particularly well-developed (Fiedler and Talley 2006; Karstensen et al. 2008; Paulmier and Ruiz-Pino 2008). In their review of the eastern tropical Pacific, Fiedler and Talley (2006) showed that the shallowest OML, with the lowest concentrations and the greatest thickness can be found in the region covered by our cruise, south of the Gulf of California. Their basin-scale review did not document mesoscale and local features related to the OML, which we follow here. In general OMLs are assumed to be formed by the combination of poor ventilation of the deep water, through import into the region by horizontal transport and by the local oxidation of particulate organics sinking from the productive surface layer. The oxidation of organic matter produces high concentrations of dissolved inorganic carbon and most inorganic nutrients in the low-oxygen waters. One question addressed by most publications about OMLs is the balance of local maintenance of low oxygen by local production and sinking of organics, and the basin-scale import of low-oxygen waters. For waters off Chile, Paulmier et al. (2006) applied inverse modeling of water mass mixing assuming oxygen to behave conservatively, then they interpreted the difference between the modeled and measured oxygen distribution as oxygen consumption. They identified the depth of the maximum oxygen gradient (oxycline) as the layer of maximum oxygen consumption. Karstensen et al. (2008) addressed the question of basin-scale import of OML waters using age estimates of the OML waters. They concluded that in general and in the region of our cruise the import of OMLs into the region is the dominant factor, but generally neither surface chlorophyll concentration nor upwelling or horizontal transport rates correlated well with the global distribution of OMLs. The hydrography in the region of the cruise is influenced by different water masses carried here by the California Current (CC) the outflow of the Gulf of California (GC) and the seasonal poleward advance of tropical waters from the Mexican Warm Pool. These waters possess contrasting hydrographic and biological properties and contribute to complicate the interpretation of our observations.

The shallow OML in the region south of the Gulf of California is in close proximity to the surface mixed layer, enhancing the possibility of vertical mixing between the OML and the upper mixed layer. For a particularly shallow OML this diapycnal mixing can be expected to leave a recognizable footprint at the local ocean surface, either as a thermal, gas concentration, or nutrient-driven chlorophyll concentration signature; for example, the surface waters above OMLs can be expected to contain elevated dissolved inorganic carbon (DIC), pCO_2, and lowered potential hydrogen (pH). These characteristics are similar to those

* Corresponding author: hmaske@cicese.mx

[1] Deceased February 2008

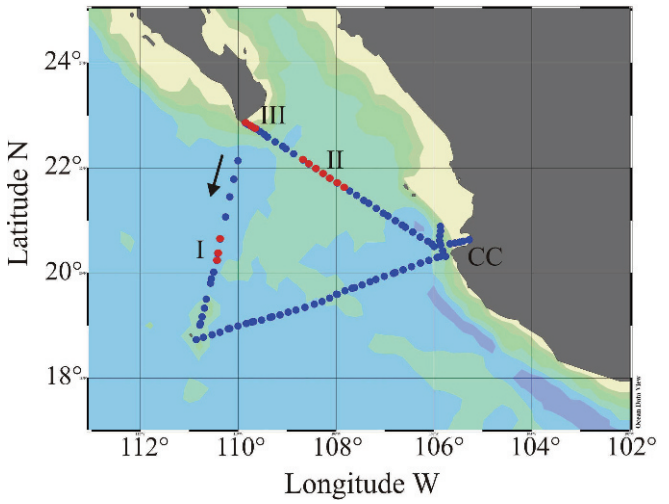

Fig. 1. Stations locations over bathymetric map. The cruise track covered a triangle between Cabo San Lucas (0 km), Isla Socorro (450 km), Cabo Corriente (CC; 1050 and 1250 km), and Cabo San Lucas (1750 km). Close to Cabo Corriente transects were added (between 1050 km and 1250 km). The beginning of the cruise sampling is indicated by the arrow. The red stations are identified below by an intrusion of subsurface California Current water; their numbers correspond to the regions marked in Fig. 9.

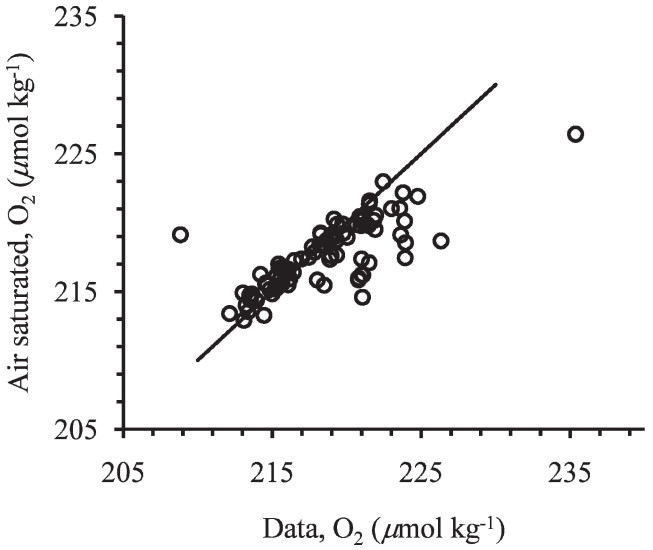

Fig. 2. The air-saturated oxygen calculated for the in situ salinity and temperature at 10-m depth compared to the CTD electrode data after applying a correction factor of 1.08. The line is the 1-to-1 relationship.

expected to be found in future surface oceans acidified by increased atmospheric pCO_2 and with all the complex changes induced by calcification dynamics, heavy metal speciation and lowered pH (Kleypas et al. 1999; Raven et al. 2005). The footprint left by vertical mixing could be modified by biological activity, for example by the conversion of some of the elevated DIC into biomass. We found little information in the literature on the characteristics of near-surface waters above a shallow OML. We intend to address this question here and started with the assumption that a significant relationship exists between the depth of the OML and concentrations of near-surface inorganic carbon and pCO_2. We also assumed that inorganic carbon and oxygen concentrations can be modified in the photic zone due to primary productivity and to the different equilibration times with air of inorganic carbon and oxygen.

Methods

The cruise on R/V *Francisco de Ulloa* (No. 0502-155) tracked the triangle between Cabo San Lucas, Isla Socorro, Cabo Corriente, and Cabo San Lucas between 28 February and 12 March 2005 (Fig. 1). At Cabo Corriente short additional tracks were added to explore the local shallow OML. The stations in red (Fig. 1) indicate profiles that demonstrate the intrusion of California Current water (*see* Results).

A conductivity–temperature–pressure profiler (CTD, SeaBird SBE9/11) equipped with redundant temperature and salinity sensors, with additional sensors for in situ chlorophyll fluorescence and oxygen was used for vertical profiling. The pycnocline for each profile was calculated from the maximum difference in σ_t over 4-m depth. It was mounted on a rosette (General Oceanics) with 12 8-liter Niskin bottles equipped with silicone rubber springs, o-rings, and tubing. The CTD sensors were calibrated in December 2004. A Clark-type oxygen electrode was attached to the CTD and calibrated at Seabird in July 2004. The oxygen electrode was not compared to chemical oxygen determinations during the cruise. We compared the oxygen concentrations ([O], μmol kg^{-1}) obtained for surface values ($<$ 10 m) by oxygen electrode with the calculated [O] assuming air saturation (Grasshoff et al. 1983). The data showed a good correlation with a regression slope indicating that the electrode gave 92.6% of the expected signal. We applied a correction factor of 1.08 to the electrode results and, consequently, the corrected surface data are very close to calculated air-saturated values (Fig. 2). A certain fraction of the data showed super-saturation and these tend to be related to higher [CHL] close to the surface. As Sarmiento and Gruber (2006) pointed out, the surface [O] are frequently oversaturated about 3% possibly caused for example by the warming of upwelled water or a misbalance of phototrophic and organotrophic processes. We possibly overcorrected the oxygen electrode data by this common oversaturation and estimated the possible errors of our saturated oxygen concentrations to be 3%; this accuracy level would affect proportionally the quantitative interpretation of the [O] data, but has no major bearing on our principal conclusions. The oxycline for each profile was calculated from the maximum difference in [O] over 4-m depth. Apparent Oxygen Utilization (AOU) was calculated using the program Ocean Data View V3.4.1 (http://odv.awi.de).

In situ light was measured with a six-spectral-channel downwelling irradiance meter (profiling reflectance radiometer, PRR 660; Biospherical Instruments) suspended from the stern A frame. An air reference instrument was mounted in the ship mast. The stern of the ship was turned

toward the sun during measurements. The instrument calculates the photosynthetically available radiation (PAR) from the six spectral channels in the visible. The 1% PAR depth was calculated in reference to the PAR within water just below the surface using the air reference to account for daylight changes during measurements.

Dissolved inorganic carbon was measured directly after samples were taken from the Niskin bottles using an automatic differential titration technique (Hernández Ayón et al. 1999) using a computer-controlled syringe pump and pH meter as described by Cajal Medrano and Maske (2005). The titration solution was 0.1 mol kg^{-1} HCl (Dilut-it, 4655-01; J. T. Baker) and the pH electrode was calibrated with commercial pH solutions (Orion). With this technique two inflexion points are obtained from the first derivative of the titration curve and the DIC concentration is calculated. The precision of our titration technique was tested, using replicates of natural samples and a standard yielding 0.4% (CV). The accuracy of the method was largely defined by the acid preparation, which is given by the company as 0.5% (CV). We used a certified reference water with known DIC and alkalinity (obtained from Scripps Institute of Oceanography, A. Dickson Lab) to check the accuracy after the cruise and obtained an overestimate of 8.5 μmol kg^{-1} corresponding to an overestimate of 0.42%. During the cruise one acid solution was prepared at the beginning of the cruise and stored in one glass bottle. This acid solution was used during the duration of the cruise for the titration and there is concern that the normality of the HCl prepared at the beginning of the cruise could have changed during the 2 weeks of the cruise.

The pCO_2 was monitored during the cruise with an infrared sensor using a Monterrey Bay Research Institute instrument for sample handling, the gas head space equilibration, standardization, and the automated instrument control (Friederich et al. 2002, 2008). The water sample was drawn continuously near the bow at 2-m depth and the air sample was taken on the second deck, sufficiently removed from the motor stack to expect negligible interference. The instrument performed without problems including the zero CO_2 calibration, but the automatic standard gas calibration failed to work. We are reporting CO_2 in Pascals (Pa) using the conversion, Pa = 0.10133 $\times$ ppm. Based on the closeness of measured air pCO_2 (38.750 $\pm$ 0.758 Pa) and the modeled climatological mean (38.684 Pa, *see* below) we assume that the accuracy of the instrument was probably better than $\pm$ 0.1 Pa. The climatological pCO_2 mean concentration during the cruise at the days, year, and latitude of the cruise of 38.684 Pa was calculated using Globalview—CO2 (2007).

In vitro chlorophyll *a* concentration [CHL] was measured on glass-fiber filtered (GFF, Whatman) samples, extracted in 90% acetone with sonication and measured fluorometrically according to Welschmeyer (1994). The Turner Design fluorometer with excitation and emission filters according to Welschmeyer was calibrated with pure chlorophyll *a* (Sigma No. C-6144). We assumed that [CHL] is the sum of monovinyl and divinyl chlorophyll *a*. The chlorophyll extracts were measured at the same time with the traditional acidification fluorometric method (Holm-Hansen et al. 1965) that yielded 12% lower chlorophyll estimates (C. Trees unpubl.). The in vitro [CHL] was used to calibrate the in situ fluorescence sensor attached to the CTD rosette. A linear response was found and the regression applied to the in situ fluorometer signal (r^2 = 0.91, df = 168). Samples obtained from the first optical depth close to the surface were grouped into daylight and nighttime data pairs; when the ratio of in situ to in vitro data was calculated, no significant difference in the ratio between the two groups was found. Therefore our in situ [CHL] data are not corrected for photoinhibition of in vivo chlorophyll fluorescence. When possible the in vitro data were used in this work; for continuous vertical chlorophyll profiles and the calculation of depth-integrated chlorophyll, the in situ data were applied.

Depth-integrated samples of zooplankton were collected by verticals hauls from 1000 m to the surface to avoid a daylight-dependent sample bias (Fiedler and Farber Lorda 2008). The 0.64-m-diameter net, 360-μm pore size, permanently open and weighted with 10-kg lead was suspended 10 m below the CTD-rosette and lowered during a hydrocast at 1 m sec^{-1}. The speed was maintained low enough that the net kept its vertical distance from the CTD as observed by the acoustic ground alarm mounted under the rosette. The net collected sample on the upcast at an average speed of 1 m sec^{-1}. The sample collected in the cod end was filtered onto one or more 45-mm-diameter glass-fiber filters (GFF Whatman) previously heated to 350°C for 2 hr and preweighed. The filtered samples were rinsed with distilled water and frozen. After drying for 24 hr at 60°C the samples were cooled in a desiccator and weighed. The empty-filter weight was subtracted from the dried-sample weight. Because of the low tow speed and the small mesh size of the net most macrozooplankters probably avoided being caught.

The reported regression statistics were significant at the $p < 0.05$ level if not otherwise reported.

Results

We projected the hydrographic properties of the three tracks into one linear section as distance over ground where the turning points for the tracks are indicated by vertical lines, thus emphasizing the general tendencies of the data (Fig. 3). Generally the vertical distribution of the oxygen concentration followed the σ_t; for example, the 122-μmol kg^{-1} oxygen band (green) followed approximately the steepest oxygen gradient, oxycline, and the 25.5 isopycnal (Fig. 3a), with a regression slope of oxycline depth vs. pycnocline depth close to 1.0 (data not shown). The data showed a shoaling of the OML and isopycnals near Cabo Corrientes between the lines marking 1000 km and 1200 km. In Fig. 3b the deep chlorophyll maximum followed approximately the depths of the pycnocline and oxycline shown in Fig. 3a and near-surface chlorophyll concentrations increased with a shallower oxycline. In Fig. 3c the salinity was graphed together with oxygen over a wider depth range including the lower OML boundary of increasing oxygen concentration [O]. In the three panels three regions can be identified with specific features. At

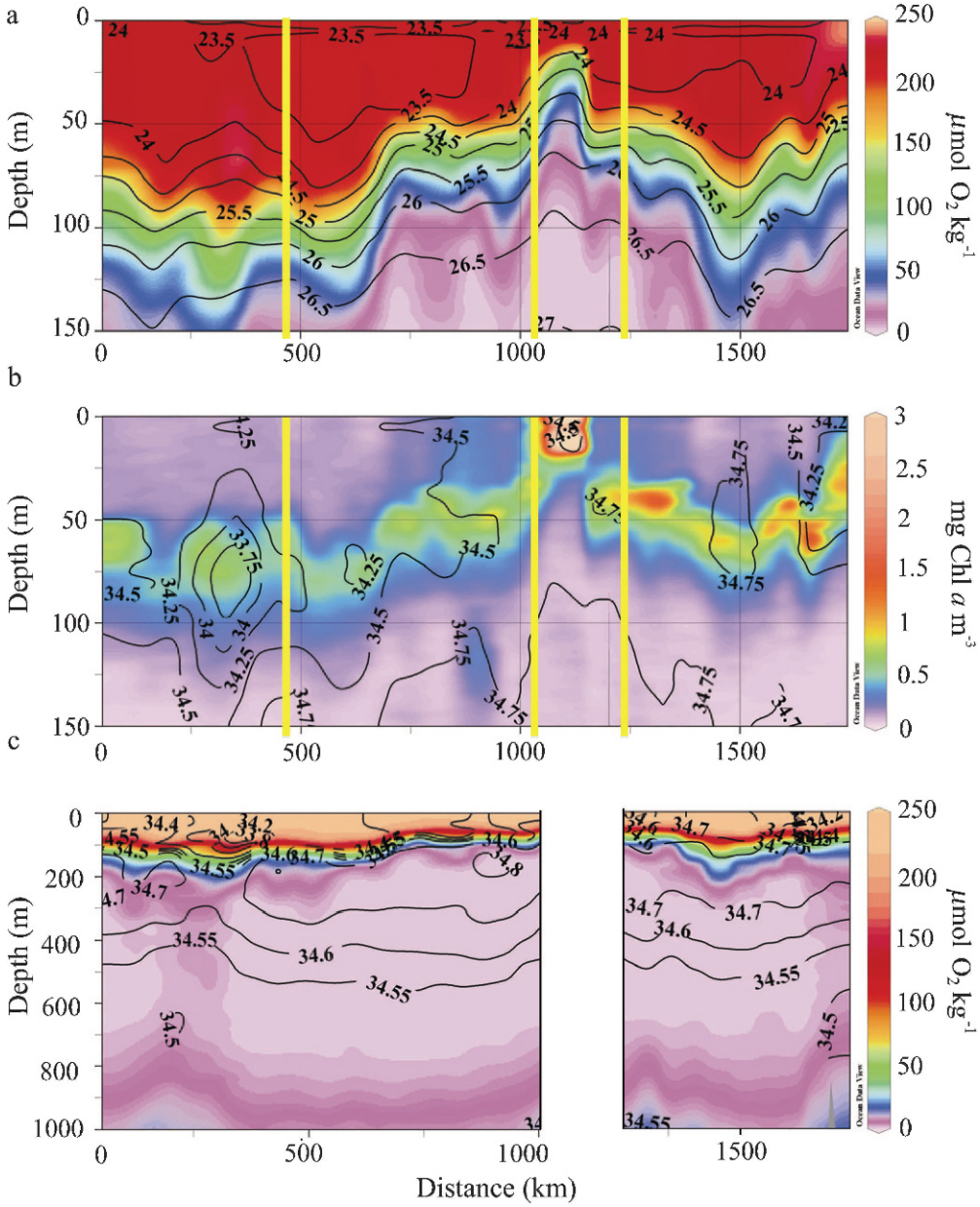

Fig. 3. Sections along the cruise transects, the transect distance is given in km. (a) Oxygen concentration (color, μmol kg^{-1}) and σ_t (lines). The yellow vertical lines correspond to the Isla Socorro (450 km), Cabo Corrientes (1050 and 1250 km). The section between 1050 km and 1250 km depicts data from additional transects close to Cabo Corrientes (*see* Fig. 1). The section is composed of 100 CTD profiles (not indicated in the section). (b) Chlorophyll concentration (color, mg m^{-3}) and salinity (lines). (c) Oxygen concentration (color, μmol kg^{-1}) and salinity (lines).The color scale of the oxygen concentration is different from panel a to spread the low concentration range. The data below 150 m are based on 41 CTD profiles.

350 km (region I) the 25.5 isopycnal rose and formed a dome (Fig. 3a), with a salinity minimum at 70 m (Fig. 3b). At 1500 km (region II) a salinity maximum at 50-m depth was accompanied by a near-surface doming of the pycnocline (Fig. 3a,b). At the end of the cruise (1700 km, region III) a weak salinity minimum was present above the oxycline.

In Fig. 4a the oxygen concentration was used to color the salinity and temperature diagram. In this figure the core of the OML is located in a narrow band with salinity above 34.5, and ranging from σ_t of 27.2 to 26 characteristic of North Pacific Intermediate Water (NPIW). Between the NPIW and the oxycline the water showed characteristics corresponding to the Subtropical Subsurface Water (StSsW), redefined as the Subtropical Underwater (STUW, O'Conner et al. 2002; Fiedler and Talley 2006). Above the oxycline most of the waters corresponded to the Equatorial Surface Water (ESW) with part of the data showing California Current Water (CCW) characteristics. In Fig. 4b the data from 0 m to 100 m from the three regions defined above in Fig. 3 were plotted to characterize their origin. The region I and II had different degrees of CCW

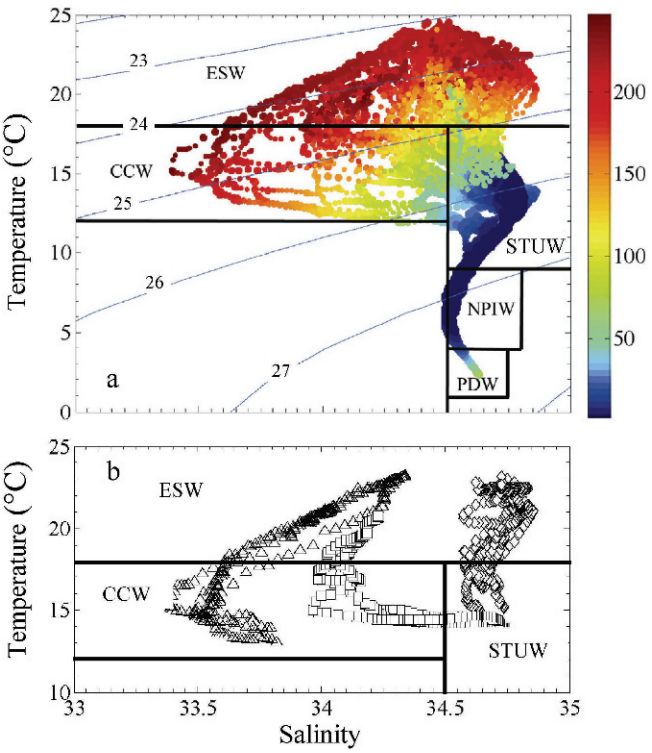

Fig. 4. Salinity and temperature vs. oxygen concentration. (a) The color band gives concentrations in μmol O_2 kg^{-1}. The OML is clearly visible as a narrow blue band of relatively high salinity and low temperature with a σ_t ranging approximately from 27 to 26. Water mass characteristics (Emery and Dewar 1982): Equatorial Surface Water (ESW), California Current Water (CCW), Subtropical Underwater (STUW), North Pacific Intermediate Water (NPIW), Pacific Deep Water (PDW). The OML with the deep salinity minimum at 34.5 corresponds to NPIW (Fiedler and Talley 2006). The maximum oxygen concentrations at the top of the data increase toward lower salinities and lower temperatures because of the increased solubility of oxygen at lower temperatures. (b) Nonconforming surface data 0 m to 100 m of the stations marked in Fig. 1: (I) triangles, (II) rhomboids, (III) squares.

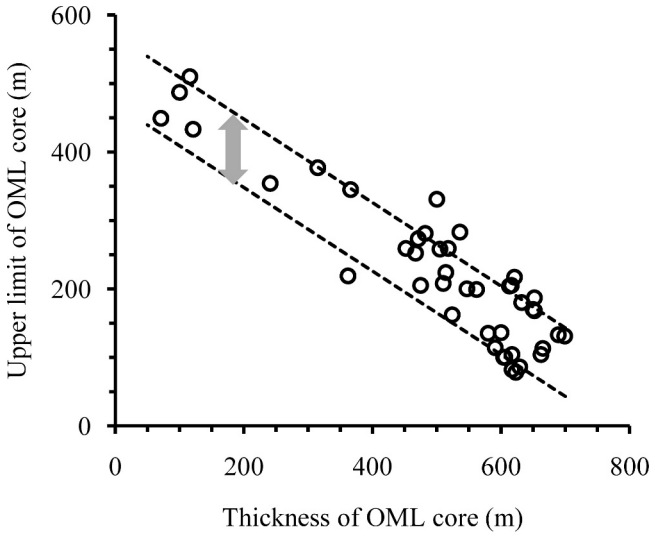

Fig. 5. The OML upper and lower depth limits were defined by a concentration just above zero (4 μmol O_2 kg^{-1}). The general tendency of the data represent the increase and decrease of the depth range of the OML, whereas the broken lines reproduce the effect of depth change of 100 m of the OML, indicated by the gray arrow. The broken lines follow the slope of the linear regression (not shown): −0.64 (r^2= 0.81, df = 38).

contribution with lowered salinities, whereas the region II showed the high salinity of Gulf of California surface waters. The data points in the upper boundary in Fig. 4a represented surface values and their color gradient (darker toward lower temperature) indicated an increase in surface [O] toward lower temperatures, consistent with the higher saturation concentration. The color bands representing concentrations above 50 μmol O_2 kg^{-1} (green to red) do not run parallel to the σ_t lines indicating a tenuous relation between [O] and the vertical density distribution (σ_t) in this concentration range.

To characterize the core of the oxygen minimum we used a boundary concentration of 4 μmol O_2 kg^{-1}; this value was chosen because it was considered to be significantly above the noise of the zero oxygen electrode signal. From the upper and lower depth limits of the core a mean depth and thickness of the core was calculated. In Fig. 5 we compare the upper depth limit of OML and the core thickness yielding a negative relation. This data pattern can be related to two processes where a major part of the shoaling of the upper limit of the OML is explained by an increase in the thickness of the OML layer leading to a slope of −0.6. A minor part of the depth change of the upper limit is due to changes in the mean depth of the OML. Both processes led to a data envelope represented by the dotted lines in Fig. 5. The gray arrow is indicating that the mean depth changed on the order of 100 m, which corresponds to the movement of the mean depth of the OML. Figure 6 shows that the lower boundary of the core followed the salinity minimum and showed constant salinities at about 34.52. In contrast, the upper boundary showed varying salinities with most data below but close to 34.8, the salinity value of the subsurface salinity maximum in the core of the Subtropical Subsurface Waters. With a narrowing of the thickness of the core, the salinity of the upper boundary approached the values of the lower boundary in a fashion that suggested the mixing of two water masses.

The measured DIC within the water column increased with depth and showed a clear relationship with [O] (Fig. 7a). Nine DIC samples out of 77 were outliers not only in Fig. 7a but also in relation to σ_t (data not shown); these outliers were eliminated from further data analysis because we considered them to be titration errors or subject to unknown process. In Fig. 7a the data from below 50-m depth resulted in a significant stoichiometry with a slope of DIC = −0.92 [O] + 2281 (r^2 = 0.86, df = 19) after eliminating the above-mentioned outliers. The intercept is suggesting a maximum DIC concentration of 2281 μmol C kg^{-1} (SE = 14) at zero oxygen. The pH at zero [O] approached 7.4 (National Bureau of Standards [NBS] scale, data not shown). The data above 50 m (Fig. 7a, empty triangles) are closely spaced at around 220 μmol O_2 kg^{-1},

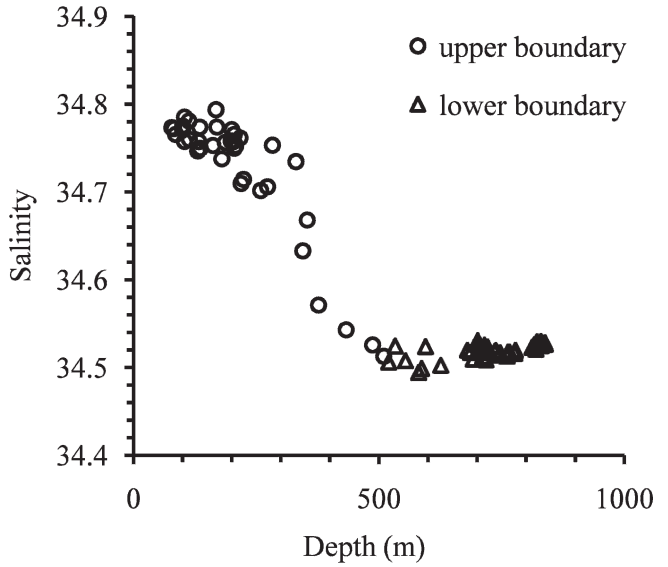

Fig. 6. The salinity at the upper border of the OML core (circles) and the lower border (triangles) vs. the depth of the respective borders. The core borders were defined by the concentration of 4 μmol O_2 kg^{-1}.

but range from 1900 μmol C kg^{-1} to 2100 μmol C kg^{-1}. In Fig. 7b DIC is regressed against apparent oxygen utilization (AOU) yielding: DIC = 0.804 × AOU + 2076 (r^2 = 0.86, df = 19).

What influence does the variable depth of the OML have on the surface mixed layer of the ocean and does it produce a characteristic signature? The most direct signal could be expected for oxygen and inorganic carbon concentration. The surface oxygen concentrations registered by the CTD electrode varied little (Fig. 7a), showed no clear relationship with OML indicators, and were close enough to theoretical air-saturated concentrations that we could use the theoretical values of saturation to adjust the electrode calibration (*see* methodology, Fig. 2). Contrary to the surface [O], the pCO_2 was related to the oxycline depth. In Fig. 8 the along-track data of pCO_2 showed mostly an inverse relationship with oxycline and pycnocline depths except for three regions identified above in Figs. 3, 4, where the relationship changed. The difference in CO_2 partial pressure between water and air ($\Delta pCO_2 = pCO_{2\text{-water}} - pCO_{2\text{-air}}$) was influenced by the depth of the oxycline (Fig. 9), where a shallower oxycline was associated with larger ΔpCO_2 and increased super-saturation in water. When the data of the nonconforming regions indicated in Figs. 4b, 9 were excluded the rest of the data adjusted to the curve in Fig. 9, indicating a tendency to super-saturation of $pCO_{2\text{-water}}$ above 92 m. At lower oxycline depth the ΔpCO_2 tended to negative values approaching −0.75. Similar statistics could be calculated for the relation of ΔpCO_2 to the pycnocline because mostly the pycnocline depth was close to the oxycline (data not shown). A comparison of Figs. 8, 9 indicated that ΔpCO_2 was forced differently in each of the nonconforming regions. Region I, where the oxycline and pycnocline depths were decoupled, did not change the statistical behavior in Fig. 9; region II

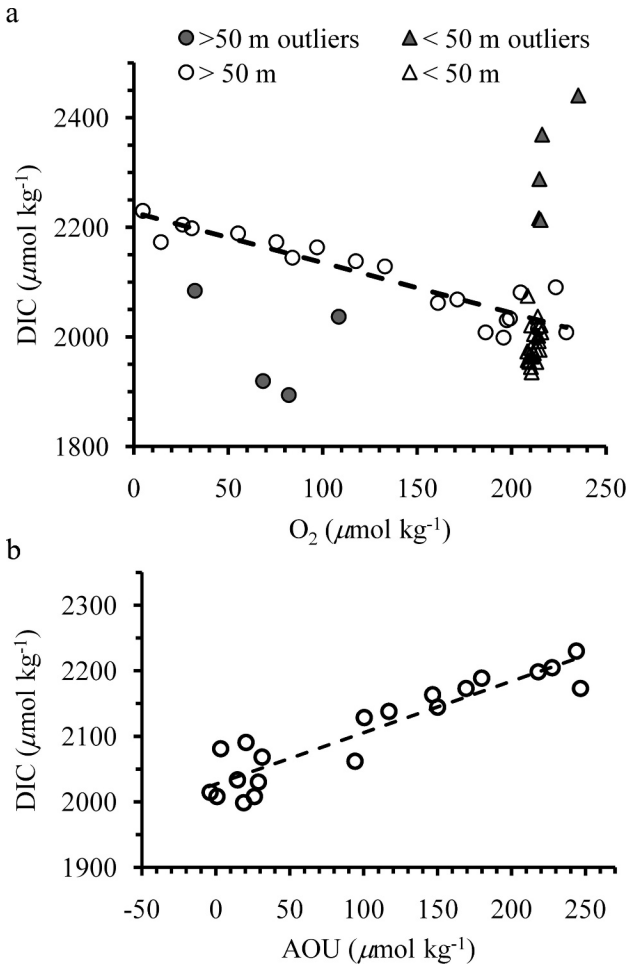

Fig. 7. (a) Dissolved inorganic carbon (DIC) vs. oxygen concentration shows a significant inverse relationship of 0.916 δDIC δO^{-1} calculated from the data below 50-m depth (circles). The DIC extrapolates to 2281 μmol kg^{-1} DIC at zero oxygen. Outliers are indicated below 50 m (filled circles) and above 50 m (filled triangles). (b) Dissolved inorganic carbon vs. the apparent oxygen utilization shows a significant molar relationship of DIC = 2027 + 0.785 × AOU (r^2 =0.86, df = 20).

led to an increase of ΔpCO_2 above the general trend, and region III to a decrease. The data trends in Fig. 9 were driven by the changes of the pCO_2 in surface waters, because the variance of pCO_2 in air was very low and had no apparent relation with the hydrography. The pCO_2 in air yielded an average value of 38.750 Pa (SD = 0.758), which was statistically not different from 38.684 Pa pCO_2, the value given by a global model for the latitude and date of the cruise (*see* Methods). For comparison, the in-water pCO_2 values at 2-m depth at the stations ranged from 37.999 Pa to 43.572 Pa (Fig. 10). These pCO_2 data and the DIC values, taken at the surface and 25-m depth, yielded a linear regression, pCO_2 = 0.0293 × DIC − 18.914 (r^2 = 0.84, df = 17; Fig. 10). From this linear regression the modeled reference value of 38.684 pCO_2 (*see* above) could be transformed into a surface DIC of 1966 μmol kg^{-1}; empirically, this DIC would represent the concentration in equilibrium with air, with the caveat that the exact pCO_2-

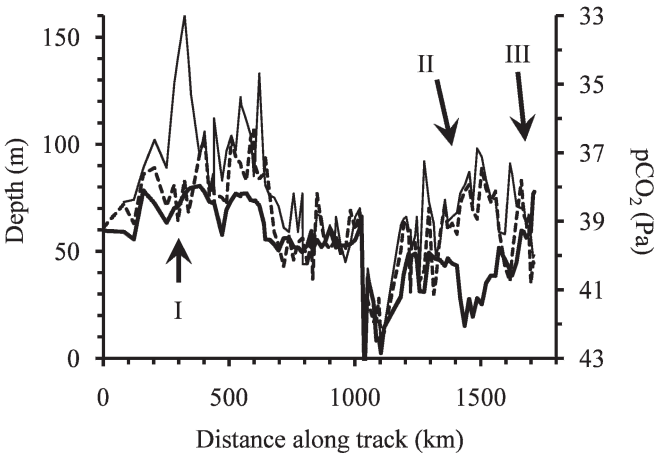

Fig. 8. Along-track traces of pycnocline depth (stippled line), oxycline depth (thin line), and pCO_2 (heavy line, inverse vertical scale). Pycnocline and oxycline represent the depths of the greatest vertical gradient in the hydrographic profiles. Three intervals of nonconforming behavior are identified, (I) around 300 km, (II) near 1500km, and (III) at the end of the track.

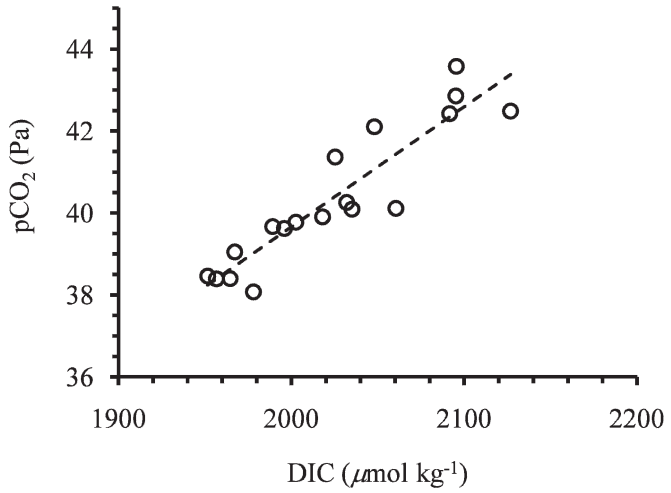

Fig. 10. The near-surface inorganic fractions DIC (circles) and pCO_2 showed a significant positive relationship with $pCO_2 = 0.0293 \times DIC - 18.914$ ($r^2 = 0.84$, df = 17). The DIC data are from the surface and 25 m, when both depths were measured the average was used.

to-DIC relationship would depend on local salinity, temperature, and pH. The values of 38.684 pCO_2 and 1966 μmol kg^{-1} DIC can be recalculated (Lewis and Wallace 1998) into the corresponding values of alkalinity (2240) and pH (8.186, NBS scale) for the average surface temperature (23.13°C) and salinity (34.48 S) during the cruise assuming a total phosphate concentration of 0.1 μmol kg^{-1} and silicate of 1 μmol kg^{-1}. The calculated alkalinity and pH values have to be considered approximations because the inorganic carbon system does not behave linearly with temperature and salinity.

Figure 11 shows a positive regression between the surface chlorophyll concentration and DIC, and as expected from Fig. 10 a similar positive relation ($p = 0.05$) was found between surface chlorophyll and pCO_2 (data not shown). We could not compare zooplankton data to DIC because we had not sufficient coincident data; therefore, in Fig. 12 the depth-integrated zooplankton biomass dry weight (ZB) was compared to the depth of 122 μmol oxygen kg^{-1} (Z_{122}), which represented the average [O] at the oxycline. The data in Fig. 12 yielded the significant exponential regression $ZB = 9.44 \times e^{(-0.018 \times Z_{122})}$ ($R^2 = 0.49$, df = 26), demonstrating that zooplankton biomass responded to a shoaling of the OML with an increase in biomass. The zooplankton data are expected to be independent of the time of day the samples were taken, because the depth range of the vertical haul exceeded the migration range of surface zooplankton. The regressions of ZB vs. the depth of the oxycline and

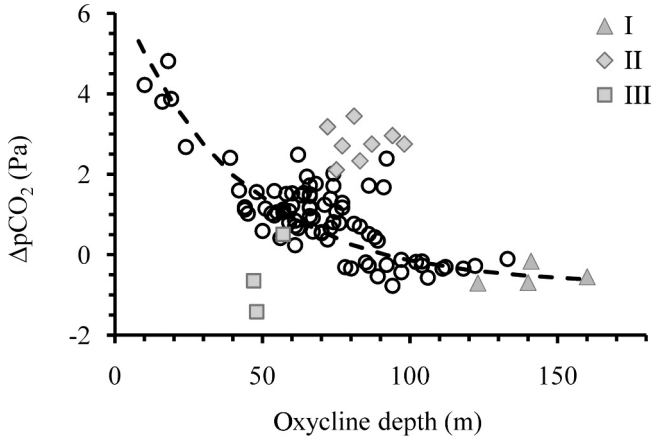

Fig. 9. The ΔpCO_2 (water minus air) vs. depth of the oxycline. The broken line is adjusted to the circles and following $\Delta pCO_2 = -0.75 + 7.4 \times e^{(\text{oxycline depth} \times -0.025)}$, ($R^2 = 0.65$, df = 91). The outliers are the same as indicated in Figs. 1, 4, and 9: filled symbols, (I) triangles, (II) rhomboids, (III) squares.

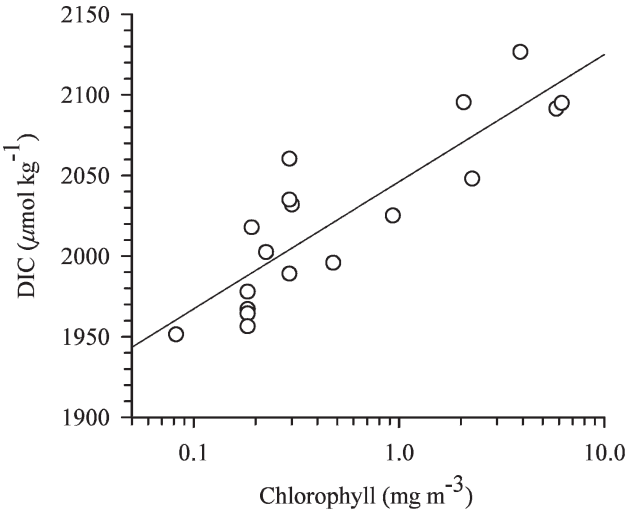

Fig. 11. Surface DIC vs. log scale, average [CHL] over the first optical depth. Dissolved inorganic carbon data were from 0-m and 25-m depths, when data from both depths were available an average value was chosen. The regression is indicated by the continuous line (*see* Eq. 1).

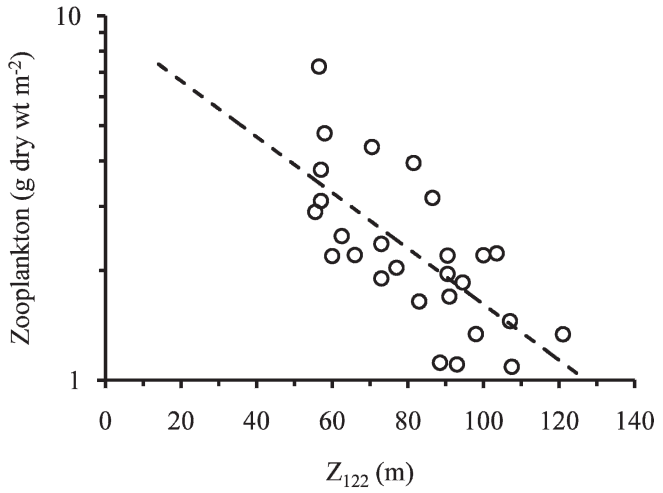

Fig. 12. Depth-integrated zooplankton (dry wt, 1000 m to surface) vs. Z_{122} the depth of 122 μmol oxygen kg^{-1}. This oxygen concentration corresponds to the average oxycline concentration and is slightly higher than half of surface oxygen concentration at typical regional salinity and temperature.

against near-surface [CHL] were both significant ($p < 0.05$), but both correlations showed lower R^2 than the data in Fig. 12. We also measured the abundance of bacteria and virus in the water column, but found no significant relationship with the variable depth of the OML or related parameters. The average bacterial abundance between 0 m and 60 m depth was 7.3×10^8 cells L^{-1}, SD = 2.8×10^8.

Discussion

In February and March 2005 we measured the regional distribution of the oxygen minimum zone south of the Gulf of California together with related inorganic carbon and biological parameters, observing an OML of variable thickness and depth of the upper border. In a sectional view the upper oxycline seemed to follow the 25.5 isopycnal (Fig. 3a) similar to the data from a basin-scale transect at 10°N discussed by Karstensen et al. (2008), but mesoscale hydrographic features modified this pattern during our cruise in three regions, indicated in Figs. 1, 3b, 4b, 9, and 10. When our regional-scale data were viewed in a salinity–temperature plot then the σ_t lines above the OML core were found to cross the color bands representing the oxygen concentration (Fig. 4a), suggesting that in this depth range the vertical transport of [O] was subject to additional mechanisms apart from turbulent exchange along isopycnals. We had defined an OML core within boundary values of 4 μmol kg^{-1}. This OML core was related to a narrow data band of well-defined salinity and temperature delimited at the bottom at ~ 700 m by a salinity minimum represented by the NPIW, also documented in the review by Fiedler and Talley (2006, their fig. 15a). The upper core of the OML was represented by the STUW with approximate salinities of 34.8. On a basin scale the OML is associated with the eastern tropical Pacific warm water pool (Fiedler and Talley 2006). In Fig. 4 the narrow band of the OML extended between the water masses NPIW and STUW. In Fig. 5 the slope between the upper limit depth of the OML core and its thickness was not −0.5, as expected for an OML that would vary its depth range symmetrically to a fixed median depth, but the value of −0.6 indicated that the upper limit of the OML varied more in depth than the lower limit.

The OML waters showed an inverse linear regression of [O] and DIC (Fig. 7a) for data below 50 m. Recalculating [O] into AOU yielded a linear relation with DIC with a slope of 0.79 (Fig. 7b); the interpretation of this slope within suboxic waters is difficult because the range of [O] would allow for different metabolic processes and because the data included two different water masses with potentially different preformed DIC concentrations (Körtzinger et al. 2001). The [O] dynamic above the oxycline did not behave conservatively; therefore, [O] in the upper 10 m showed no relation with OML indicators like the depths of the OML core or the oxycline, but seemed to be approximately in equilibrium with air (Fig. 2). The near-surface pCO_2 related negatively with indicators of the water column structure, the oxycline and pycnocline depths, except in three regions (Fig. 8) in region I the oxycline was lower than expected, in region II the pCO_2 was higher and in region III lower than expected. These three regions demonstrated that for the broad region of the entire cruise pCO_2 followed general tendencies, but local water mass information would still be necessary to interpret the data. A comparison of Figs. 4b, 9 indicated that for Gulf of California water (rhomboid symbols) the higher than expected ΔpCO_2 would be associated with its high surface salinities. Following the general data trend in Fig. 9 an oxycline depth of < 92 m would indicate a significant increase of pCO_2 in surface waters with the exception of region III (*see* Fig. 8). Above we showed that inorganic carbon concentration near the surface responded to the depth of the OML but [O] did not; this difference has been noted before (Sarmiento and Gruber 2006), and was probably related to the slower equilibration of inorganic carbon with the atmosphere compared to oxygen.

Figure 11 demonstrated the semi-logarithmic regression of DIC with surface chlorophyll concentration yielding

$$\mathrm{DIC} = 2046.2 + 34.27 \times \ln([\mathrm{CHL}]),\ R^2 = 0.75,\ \mathrm{df} = 17 \quad (1)$$

Depth-integrated zooplankton biomass (ZB, g dry wt m^{-2}) probably also increased with DIC (although we had not enough coincident data to demonstrate it statistically), but Fig. 12 indicates a significant relation of ZB with the Z_{122}, the depth of the average [O] in the oxycline (122 μmol kg^{-1}, *see* Results). Therefore ZB can be expected to increase with surface DIC concentrations above a shallow OML similar to [CHL]. The link between the biomass indicators ([CHL], ZB) and DIC in surface waters can be explained by the concomitant transport of DIC and inorganic nutrients from the OML toward the surface, the inorganic nutrients supporting increased primary production. How to explain the semi-log relationship between DIC and [CHL]? Consider that the surface layer is in equilibrium and that 1961 μmol C kg^{-1} is the empirical DIC concentration that is in equilibrium with air (cf. Fig. 10 and Results) and any

DIC concentration above would have been a result of mixing OML water into the surface. Part of the DIC would be converted into organic carbon by primary production. Here we only considered particulate organic carbon concentration ([POC], μmol kg^{-1}) without dissolved organic carbon, which we assumed to maintain a steady concentration at all DIC. The [CHL] concentration has an empirical nonlinear relationship with particulate organic carbon (mg m^{-3}; Legendre and Michaud 1999); here, we used their relationship for data < 200-m depth. We applied a correction factor (W, 0.88) to the chlorophyll concentration to adjust our [CHL] data obtained with the Welschmeyer method to the lower values obtained with the traditional fluorometric method used by Legendre and Michaud (*see* Results). Also the POC was converted to molar concentration (μmol kg^{-1}) by dividing by seawater density (D) and the molecular weight of carbon (MW).

$$\mathrm{POC} = \mathrm{D}^{-1} \times \mathrm{MW}^{-1} \times 10^{(2.291 + 0.353 \times \log[\mathrm{CHL} \times \mathrm{W}])} \quad (2)$$

The sum of POC and DIC would represent in large part the inorganic carbon mixed into surface waters; missing is the inorganic carbon that was ventilated to the air (*see* below). When POC calculated according to Eq. 2 was regressed against the sum of DIC and POC, a significant ($R^2 = 0.75$, df = 18) linear relationship (Fig. 13) was found:

$$\mathrm{DIC} + \mathrm{POC} = 6.3 \times \mathrm{POC} + 1959 \quad (3)$$

Therefore about 16% of the imported inorganic carbon appears as POC. This rough estimation did not consider the following mechanisms that might have influenced the quantitative estimate and also the interpretation: (1) The dissolved organic carbon was not considered, because we assumed it invariant at different [CHL] concentrations; (2) The ventilation of inorganic carbon to the atmosphere (C_v) would increase the sum of inorganic carbon imported from the OML (left side of Eq. 3) to DIC + POC + Cv. Note that C_v (μmol C kg^{-1}) is here assumed to be the time-integrated inorganic carbon that was ventilated and would be proportional to DIC − 1961. If C_v would be included in Eq. 3 then the ratio of POC to total inorganic carbon transported into the surface layer would be smaller; hence, a smaller proportion of that inorganic carbon would be available to feed the biological pump; (3) The stoichiometry between DIC and inorganic nutrients that forms the link between organic carbon production and DIC probably does not follow the Redfield ratio. In OMLs the stoichiometry between C : N is increased due to denitrification and ammonium oxidation, and this would lead to changes in the POC-to-DIC relationship (Farias et al. 2007); (4) The dependence of the carbon on nutrient stoichiometry might lead to greater organic standing stock than considered here, because increased in situ pCO_2 has been reported to increase the ratio of carbon to other nutrients in organic material (Riebesell et al. 2007), possibly leading to a higher POC : Chl *a* ratio above a shallow OML than under global pCO_2 concentration; (5) The above estimate was based on near-surface concentrations without considering depth-integrated values of the surface mixed layer. Because the near-surface DIC (cf. Fig. 9) and [CHL] values covary with the depth of the pycnocline, the above approach should be confirmed using depth-integrated data from the surface mixed layer; (6) A closer understanding of the carbon exchange between the surface layer and the OML would include the inorganic ballast that modifies the efficiency of the biological pump and, hence, the balance of DIC to Chl *a*. Related to this is the effect of decreasing pH on the calcium carbonate saturation state in an anoxic OML (Feely et al. 2008).

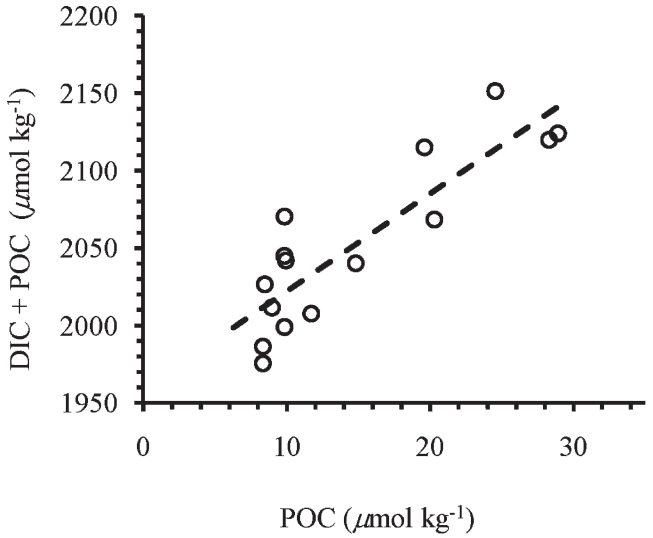

Fig. 13. Surface POC calculated from [CHL] vs. the sum of DIC and POC.

The above explanation for the covariation of DIC and Chl *a* was based on the argument that DIC transport into the surface layer implied the concomitant transport of inorganic nutrients. An alternative explanation for the covariation of DIC and Chl *a* could be based on the negative relation of DIC vs. depth of pycnocline and the light limitation of phytoplankton controlled by the depth of the pycnocline. If the primary production would have been inhibited by a surface mixed layer extending well below the bottom of the euphotic zone as conceptualized in the Sverdrup (1953) model, then a shallower oxycline could have provided more DIC and inorganic nutrients and at the same time would have favored the primary production because the bottom of the euphotic zone would have been at the depth of, or below the pycnocline. We tested this alternative hypothesis by comparing the depth of the pycnocline with the 1% light depth calculated from the depth-integrated chlorophyll concentration (Morel and Maritorena 2001). First we compared the calculated depth of the euphotic zone with radiometric data and arrived at a good correspondence of the calculated with the measured 1% light depth (slope = 0.93, $r^2 = 0.74$, $n = 8$) and then calculated the euphotic depths for the rest of the stations. The ratio of euphotic depth to pycnocline depth varied between 0.5 and 1.5 without a significant trend with the depth-integrated chlorophyll or surface [CHL]. On the other hand the depth of the deep chlorophyll maximum followed mostly the depth of the oxycline and the depth of the 1% light depth implying that the primary production

had arrived at a steady state of primary production, nutrient supply, and light attenuation. Therefore this alternative hypothesis did not explain the covariation of DIC and [CHL], leading us to our original conclusion that the concomitant transport of DIC and inorganic nutrients led to the greater availability of the latter, which fuelled the increased [CHL] production.

Above we estimated that a major part of the DIC transported into the surface layer was changed into POC and, thus, was available to support the biological pump (Eq. 3), which implied a major role of sinking organic carbon in maintaining the OML. The question of the relative importance of locally produced vs. imported oxygen minimum below the pycnocline has been addressed in the literature before. For the oxygen minimum in the Humboldt Current, Paulmier et al. (2006) approached the question by modeling of the transport and mixing of the water masses with a hydrographic model. They considered oxygen as a conservative tracer of the water masses and interpreted the difference to the observed distribution of oxygen as local rates of oxygen consumption. These authors considered the local oxygen consumption at and below the pycnocline to be a significant mechanism in maintaining the OML, suggesting that the organic carbon transported from the surface layer toward the OML played a significant role in the maintenance of the OML. This conclusion by Paulmier et al. (2006) is in agreement with our estimate in Eq. 3, although their results were based on the oxygen balance whereas ours were based on the carbon balance and we had found different responses of oxygen and inorganic carbon above the pycnocline. For example, we found no relation of the surface oxygen concentrations with the depth of the oxycline, but oxygen was close to air saturation contrary to the inorganic carbon.

For the region and the period of the cruise the upper boundary of the OML varied sufficiently to leave a clear signature at the surface in inorganic carbon or phytoplankton concentration (Fig. 9); also, surface temperature at 1-m and 3-m depth increased significantly with a higher OML core (data not shown). One possible explanation for the unexpected negative relationship of OML depth with surface temperature might be that surface heating of the water dominated over the contribution of low-temperature OML water close to the surface. We found no significant relationship of surface temperature with other hydrographic parameters or with surface pCO_2, similar to Goyet and Peltzer (1997), which makes the interpretation of remotely sensed sea-surface temperature as a proxy for pCO_2 not feasible. Contrary to Goyet and Peltzer (1997), we did not find a diurnal sea-surface pCO_2 oscillation.

Our data suggest that the shallow oxygen minimum layer supported an increased primary and secondary production by increasing the transport of inorganic nutrients into the euphotic zone. The resulting increased biomass might then partially sink into the OML where it might be partially remineralized and, thus, help to maintain the presence of the OML.

Acknowledgments

We thank Stephen V. Smith and Aurelien Paulmier for detailed and constructive reviews of an earlier version of the manuscript. The manuscript improved significantly with the suggestions of two anonymous reviewers. The intensive data collection was made possible by the dedicated help of all scientific and technical participants of the cruise *Francisco de Ulloa*-0502-155. Chlorophyll was measured at the Center for Hydro Optics and Remote Sensing/San Diego State University. The cruise was financed by the Consejo Nacional de Ciencia y Tecnología grant 38834-T.

References

Cajal Medrano, R., and H. Maske. 2005. Growth efficiency and respiration at different growth rates in glucose-limited chemostats with natural marine bacteria populations. Aquat. Microb. Ecol. **38:** 125–133.

Chan, F., J. A. Barth, J. Lubchenko, A. Kirincich, H. Weeks, W. T. Peterson, and B. A. Menge. 2008. Emergence of anoxia in the California current large marine ecosystem. Science **319:** 920.

Diaz, R. J., and R. Rosenberg. 2008. Spreading dead zones and consequences for marine ecosystems. Science **231:** 927–929.

Emery, W. J. K., and J. S. Dewar. 1982. Mean temperature–salinity, salinity–depth and temperature–depth curves for the North Atlantic and the North Pacific. Prog. Oceanogr. **11:** 219–305.

Farias, L., A. Paulmier, and M. Gallegos. 2007. Nitrous oxide and N-nutrient cycling in the oxygen minimum zone off northern Chile. Deep-Sea Res. I **54:** 164–180.

Feely, R. A., C. L. Sabine, J. M. Hernandez-Ayon, D. Ianson, and B. Hales. 2008. Evidence for upwelling of corrosive 'acidified' water onto the continental shelf. Science **320:** 1490–1492.

Fiedler, P. C., and J. Farber Lorda. 2008. Zooplankton night–day ratios and the oxygen minimum layer in the eastern Pacific. NOAA Technical Memorandum NOAA-TM-NMFS-SWFSC-424.

———, and L. D. Talley. 2006. Hydrography of the eastern tropical Pacific: A review. Prog. Oceanogr. **69:** 143–180.

Friederich, G. E., J. Ledesma, O. Ulloa, and F. P. Chavez. 2008. Air–sea carbon dioxide fluxes in the coastal southeastern tropical Pacific. Prog. Oceanogr. **79:** 156–166, doi:10.1016/j.pocean.2008.10.001.

———, P. M. Walz, M. G. Burczynski, and F. P. Chavez. 2002. Inorganic carbon in the central California upwelling system during the 1997–1999 El Niño–La Niña event. Prog. Oceanogr. **54:** 185–203.

Globalview—CO_2. 2007. Cooperative data integration Project—Carbon dioxide. CD-ROM. Boulder (CO): NOAA. Available from http://www.esrl.noaa.gov/gmd/ccgg/globalview/.

Goyet, C., and E. T. Peltzer. 1997. Variation of CO_2 partial pressure in surface seawater in the equatorial Pacific Ocean. Deep-Sea Res. I **44:** 1611–1625.

Grasshoff, K., M. Ehrhardt, and K. Kremling. 1983. Methods of seawater analysis, 2nd ed. Verlag Chemie.

Hernández Ayón, M. J., S. Belli, and A. Zirino. 1999. pH, alkalinity and total CO_2 in coastal seawater by potentiometric titration with a difference derivative readout. Anal. Chim. Acta **394:** 101–108.

Holm-Hansen, O., C. J. Lorenzen, R. W. Holmes, and J. D. H. Strickland. 1965. Fluorometric determination of chlorophyll. J. Cons. Cons. Int. Explor. Mer. **30:** 3–15.

Karstensen, J., L. Stramma, and M. Visbeck. 2008. Oxygen minimum zones in the eastern tropical Atlantic and Pacific oceans. Prog. Oceanogr. **77:** 331–350.

Kleypas, J. A., R. W. Buddemeier, D. Archer, J. P. Gattuso, C. Langdon, and B. N. Opdyke. 1999. Geochemical consequences of increased atmospheric carbon dioxide on coral reefs. Science **284:** 5411, doi:10.1126/science.284.5411.118.

Körtzinger, A., J. I. Hedges, and P. D. Quay. 2001. Redfield ratios revisited: Removing the biasing effect of anthropogenic CO_2. Limnol. Oceanogr. **46:** 964–970.

Legendre, L., and J. Michaud. 1999. Chlorophyll *a* to estimate the particulate organic carbon available as food to large zooplankton in the euphotic zone of oceans. J. Plankton Res. **21:** 2067–2083.

Lewis, E., and D. W. R. Wallace. 1998. Program developed for CO_2 system calculations, ORNL/CDIAC-105. Carbon Dioxide Information Analysis Center, Oak Ridge National Laboratory, U.S. Department of Energy.

Morel, A., and S. Maritorena. 2001. Bio-optical properties of oceanic waters: A reappraisal. J. Geophys. Res. **106:** 7163–7180.

O'Conner, B. M., R. A. Fine, K. A. Maillet, and D. B. Olson. 2002. Formation rates of subtropical underwater in the Pacific Ocean. Deep-Sea Res. I **49:** 1571–1590.

Oschlies, A., K. G. Schulz, U. Riebesell, and A. Schmittner. 2008. Simulated 21st century's increase in oceanic suboxia by CO_2-enhanced biotic carbon export. Glob. Biogeochem. Cycles **22:** GB4008, doi:10.1029/2007GB003147.

Paulmier, A., and D. Ruiz-Pino. 2008. Oxygen minimum zones (OMZs) in the modern ocean. Prog. Oceanogr. **80:** 113–128, doi:10.1016/j.pocean.2008.08.001.

———, ———, V. Garcon, and L. Farias. 2006. Maintaining of the east south pacific oxygen minimum zone (OMZ) off Chile. Geophys. Res. Let. **33:** L20601, doi:10.1029/2006GL026801.

Raven, J., and others. 2005. Ocean acidification due to increasing atmospheric carbon dioxide. The Royal Society, policy document 12/05.

Riebesell, U., and others. 2007. Enhanced biological carbon consumption in a high CO_2 ocean. Nature **450:** 545–548, doi:10.1038/nature06267.

Sarmiento, J. L., and N. Gruber. 2006. Ocean biogeochemical dynamics. Princeton Univ. Press.

Sverdrup, H. U. 1953. On conditions for the vernal blooming of phytoplankton. J. Cons. Cons. Int. Explor. Mer **18:** 287–295.

Welschmeyer, N. A. 1994. Fluorometric analysis of chlorophyll *a* in the presence of chlorophyll *b* and pheopigments. Limnol. Oceanogr. **39:** 198–1992.

Associate editor: Robert R. Bidigare

Received: 27 March 2009
Accepted: 17 September 2009
Amended: 18 October 2009